Research Square

Preprints are preliminary reports that have not undergone peer review.
They should not be considered conclusive, used to inform clinical practice,
or referenced by the media as validated information.

Spatiotemporal Evolution of Combined Heat and Drought Hazard for Spring Maize in the Hilly Region of Southwest China

Yang Yang
Sichuan University
Lu Zhao
luya1121@163.com

Sichuan University
Shouzheng Jiang
Sichuan University
Cun Zhan
Kunming University of Science and Technology
Ningbo Cui
Sichuan University
Yufang Zhang
Environment-friendly and Efficient Water-Saving Technology and Equipment for Hilly Agriculture Key Laboratory of Sichuan Province
Ziyi Liu
Sichuan University
Ziqi Song
Sichuan University
Hanyue Li
Sichuan University

Research Article

Keywords: Combined heat and drought events, Maize, Hazard assessment, Spatiotemporal differentiation, Hilly regions of Southwest China

Posted Date: November 25th, 2026

DOI: https://doi.org/10.21203/rs.3.rs-11689122/v1

License: This work is licensed under a Creative Commons Attribution 4.0 International License.
Read Full License

Additional Declarations: No competing interests reported.

Spatiotemporal Evolution of Combined Heat and Drought Hazard for Spring Maize in the Hilly Region of Southwest China

Yang Yang[a], Lu Zhao[a*], Shouzheng Jiang[a], Cun Zhan[b], Ningbo Cui[a], Yufang Zhang[c], Ziyi Liu[a], Ziqi Song[a], Hanyue Li[a]

a. State Key Laboratory of Hydraulics and Mountain River Engineering & College of Water Resource and Hydropower, Sichuan University, Chengdu, 610065, China.

b. Faculty of Electric Power Engineering, Kunming University of Science and Technology, Kunming, 650500, China.

c. Environment-friendly and Efficient Water-Saving Technology and Equipment for Hilly Agriculture Key Laboratory of Sichuan Province, Chengdu, 610066, China.

*Corresponding author:

State Key Laboratory of Hydraulics and Mountain River Engineering & College of Water Resource and Hydropower, Sichuan University, Chengdu, 610065, China.

Email: luya1121@163.com (L. Zhao)

Tel: +86-13688397865

Acknowledgments

This study was supported by the National Key Research and Development Program of China (2024YFD2301305) and the National Natural Science Foundation of China (52109060).

Abstract:

As the climate warms, combined heat and drought events (CHDE) pose an increasing threat to rain-fed maize production. This study developed a daily-scale hazard assessment framework to characterize CHDE hazard for spring maize in the hilly region of Southwest China from 1961 to 2023. The framework integrated the standardized precipitation requirement index (SPRI), excessive degree days (EDD), antecedent drought and heat factors, and a copula-based duration–severity model to assess temporal evolution and spatial differentiation across maize growth stages. Results showed that drought-related antecedent stress dominated throughout the growing season, accounting for more than 69% of the total antecedent-stress contribution. CHDE duration, severity, and the integrated hazard index peaked from grain filling to physiological maturity. Compared with 1961–1992, CHDE during 1993–2023 occurred more frequently, lasted longer, and exhibited greater severity and higher hazard, while high-hazard areas expanded westward from the eastern part of the study area. This study enhanced the mechanistic understanding of compound stress dynamics and provided a scientific basis for stage-specific adaptation strategies in rain-fed maize systems across the hilly regions of Southwest China.

Keywords: Combined heat and drought events; Maize; Hazard assessment; Spatiotemporal differentiation; Hilly regions of Southwest China.

1. Introduction

Over the past century, the global climate has warmed significantly (Guo et al. 2022). This trend has led to more frequent and intense extreme weather events, such as heatwaves and droughts, occurring across different regions and periods (Bolan et al. 2024; Xu et al. 2023). These events posed a serious threat to agricultural production (Vogel et al. 2019). Extreme weather impacted food security mainly through crop responses to variations in temperature and precipitation. Heatwaves and droughts were the primary drivers of reductions in crop yield. Of particular concern were combined heat and drought events (CHDE) (Zhu et al. 2021a; Riedesel et al. 2024). The cumulative stress from both events often resulted in greater yield losses than when each occurs separately (Zhu et al. 2021b). Research indicated that the severity of CHDE in global farmland during the growing season was intensifying. The affected cultivated area was expected to expand to approximately 2-5.7 million km^2 (Wang et al. 2023a; Yu et al. 2024; Liu et al. 2024). As a result, CHDE have become a major challenge to food security.

Risk assessment of extreme climate events was essential for identifying potential impacts of climate change and for developing targeted mitigation and adaptation strategies (Wang et al. 2025). In agriculture,

assessing the risks of climate-related disasters was crucial for ensuring food security and reducing the vulnerability of agricultural production. The first step in risk assessment was hazard assessment, which focused on identifying and analyzing the driving factors of climate-related agricultural disasters. This was typically done by quantifying the product of the probability and severity of disaster occurrences (Chen et al. 2024; Hao et al. 2022). This methodology effectively quantified the potential threats of extreme climate events to crop production and has been validated by multiple studies as an effective tool for risk management (Zhi et al. 2024).

Maize, one of the world's three major staple crops, plays an important role in global food security (Liu 2024; Wang et al. 2018b). However, as a C4 crop, maize is highly sensitive to climate change. Its growth and development are closely linked to temperature and precipitation, making it extremely vulnerable to CHDE (Liu et al. 2025; Li et al. 2025). Studies suggested that CHDE significantly increased the risk of a reduction in maize yield compared to isolated heat or drought events (Feng et al. 2021). CHDE can substantially increase the probability of maize yield reductions compared with drought or heat alone (Feng et al. 2019). Furthermore, CHDE were becoming the primary form of heat-drought stress affecting maize (He et al. 2024).

In recent years, research on CHDE has made some progress, primarily focusing on its basic characteristics, such as frequency and severity. However, understanding of its spatiotemporal dynamics and driving mechanisms remained limited (Liu et al. 2022; Li et al. 2021). The duration and specific timing of CHDE's onset and termination were crucial for crop growth (Yu et al. 2024). Existing drought indices were mainly designed for longer time scales, such as monthly or annual (Zhang et al. 2023b; Yang et al. 2025). As a result, current studies typically characterized CHDE in monthly or annual units or treated it as heat stress superimposed on long-term drought conditions (Wu et al. 2024; Zhou et al. 2025; Shi et al. 2024). Such long-scale indicators hindered detailed analysis at the daily level, limiting the understanding of drought-heat interactions. They also failed to capture short-term CHDE, which can last only a few days but is becoming increasingly frequent. Even brief CHDE during critical stages of maize growth, such as emergence or pollination, can lead to severe yield losses (Luan and Vico 2021; Wang et al. 2023b). Maize is sensitive to both water and heat stress, making it particularly vulnerable under compound stresses. Drought can reduce maize resilience beyond the stress period, while warm early-season conditions can increase sensitivity to subsequent heat (Jing et al. 2023; Hamed et al. 2025). Most research focused on the direct impacts of CHDE, often overlooking the cumulative and delayed

effects of prior extreme weather. Therefore, when using composite indices to assess CHDE severity across maize growth stages, it was necessary to consider the effects of antecedent drought and heat exposure.

This study investigated spring maize using a daily standardized precipitation requirement index (SPRI) as a drought indicator and excessive degree days (EDD) as a heat stress indicator. It combined an improved composite intensity index (which incorporated an antecedent factor to reflect pre-event stress) with copula functions to calculate the occurrence probability of CHDE, thereby constructing a hazard assessment model for CHDE damage. The objectives were to (1) characterize drought and heat stress and their antecedent factors across maize growth stages to clarify the background conditions of CHDE; (2) investigate the occurrence patterns and spatiotemporal evolution of CHDE during each stage of maize growth; (3) evaluate CHDE hazard and its temporal variability to identify critical growth stages and high-hazard regions. The findings can provide support for growth-stage-specific maize management and water-resource allocation in the hilly regions of Southwest China.

2. Study area and methods

2.1 Study area

The Central Sichuan (CSC) Hills (E: 102.82°−108.54°; N: 27.66°−33.04°) are a typical hilly region in Southwest China (Chen et al. 2013; Kumwimba et al. 2016). The area exhibits a subtropical monsoon climate, with an average annual temperature of 17.5 °C and average annual precipitation of approximately 1000 mm. Precipitation is concentrated in summer and autumn, influenced by monsoons and topography, while it is scarce in winter and spring (Zhu et al. 2009). The CSC Hills are a major maize-producing region in Southwest China. However, the reliance on rain-fed agriculture makes the ecosystem highly sensitive to climate change. In addition, intensified global warming exacerbates circulation anomalies, leading to more frequent heat events (Chen et al. 2018; Yu et al. 2023; Lin et al. 2022). The growing season for spring maize (April-August) overlapped with the peak period for heat-drought events, severely constraining maize production and threatening food security (Zhang et al. 2023a). Based on the historical development and current status of maize cultivation in the CSC Hills, the region was divided into five zones (Fig 1): (I) Southern Basin Hills; (II) Eastern Ridges and Valleys; (III) Peripheral Mountains; (IV) Western Basin Flat Hills; and (V) Central Basin Low Hills.

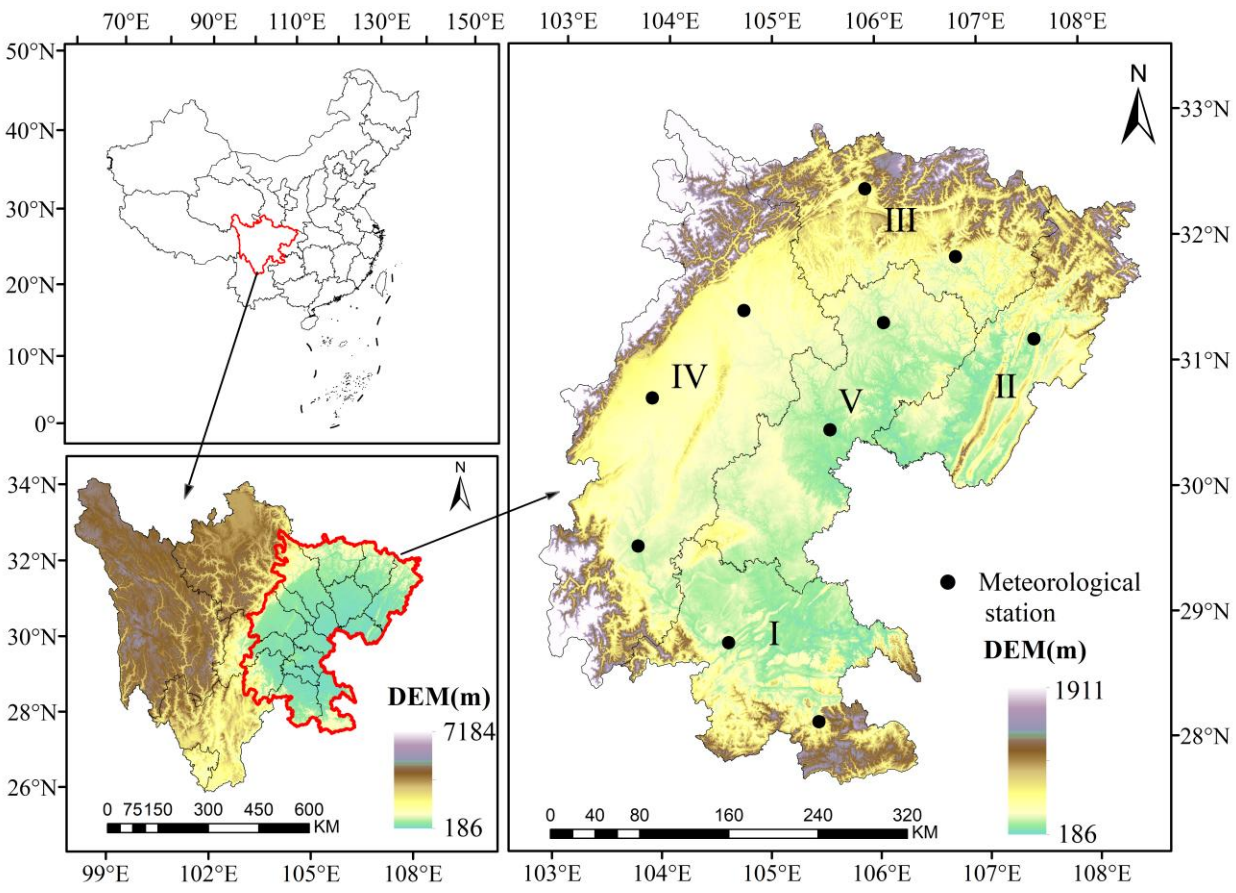

Fig 1. Study Area and Meteorological Station Distribution.

2.2 Dataset

This study primarily used phenological records for spring maize and daily meteorological data from the CSC Hills. The meteorological data were sourced from the China Meteorological Data Service Center (http://data.cma.cn) and covered the period from 1961 to 2023. The data included maximum temperature (T_{max}), minimum temperature (T_{min}), precipitation (P), relative humidity (RH), sunshine duration (n), and wind speed at 2 m (u_2). To ensure data reliability and account for the topography of the study area, ten representative stations in the CSC Hills were selected. Missing data were filled using linear interpolation. The phenological data were compiled from provincial statistical yearbooks and published studies. Based on comprehensive calculations and analysis, the specific growth stages of maize are detailed in Table 1. Crop coefficients (K_c) for the maize growing season were referenced from Wang (2012), which focused on drought characteristics during growth stages of maize in the Sichuan Basin, with specific values presented in Table 2.

122 **Table 1.** Growth Stage Classification of Spring Maize in the CSC Hills.

Growth stage	Description	Time
V0-VE	Sowing to Seedling	Early April to mid-April
VE-V6	Seedling to Jointing	Mid-April to late May
V6-R1	Jointing to Tasseling	Early June to late June
R1-R3	Tasseling to Grain filling	Early July to mid-to-late July
R3-R6	Grain filling to Physiological maturity	Mid-to-late July to mid-to-late August

123 **Table 2.** Crop Coefficients for Spring Maize in the CSC Hills.

Region	April	May	June	July	August
I	0.8	1.2	1.35	1.25	1.05
II	0.8	1.2	1.35	1.25	1.05
III	0.65	1.05	1.25	1.3	1.2
IV	0.7	1.1	1.3	1.4	1.25
V	0.8	1.1	1.4	1.3	1.12

124 ## 2.3 Methods

125 Fig 2 summarizes the hazard framework, which consists of four components. First, daily-scale SPRI
126 and EDD were used to identify drought and heat events, respectively. Second, drought and heat intensities
127 were transformed into probability-based measures to eliminate differences in units and magnitude. These
128 measures were then integrated with antecedent stress factors to identify and characterize CHDE.
129 According to the type of antecedent stress, the identified events were further classified as
130 drought-preconditioned CHDE (CHDEd) and heat-preconditioned CHDE (CHDEh). Third, a
131 copula-based duration–severity model was used to estimate CHDE occurrence probability. Fourth, CHDE
132 hazard was quantified by combining occurrence probability with event magnitude. Interperiod
133 comparisons and time–frequency analyses were subsequently conducted. The following subsections
134 describe the calculations for each component.

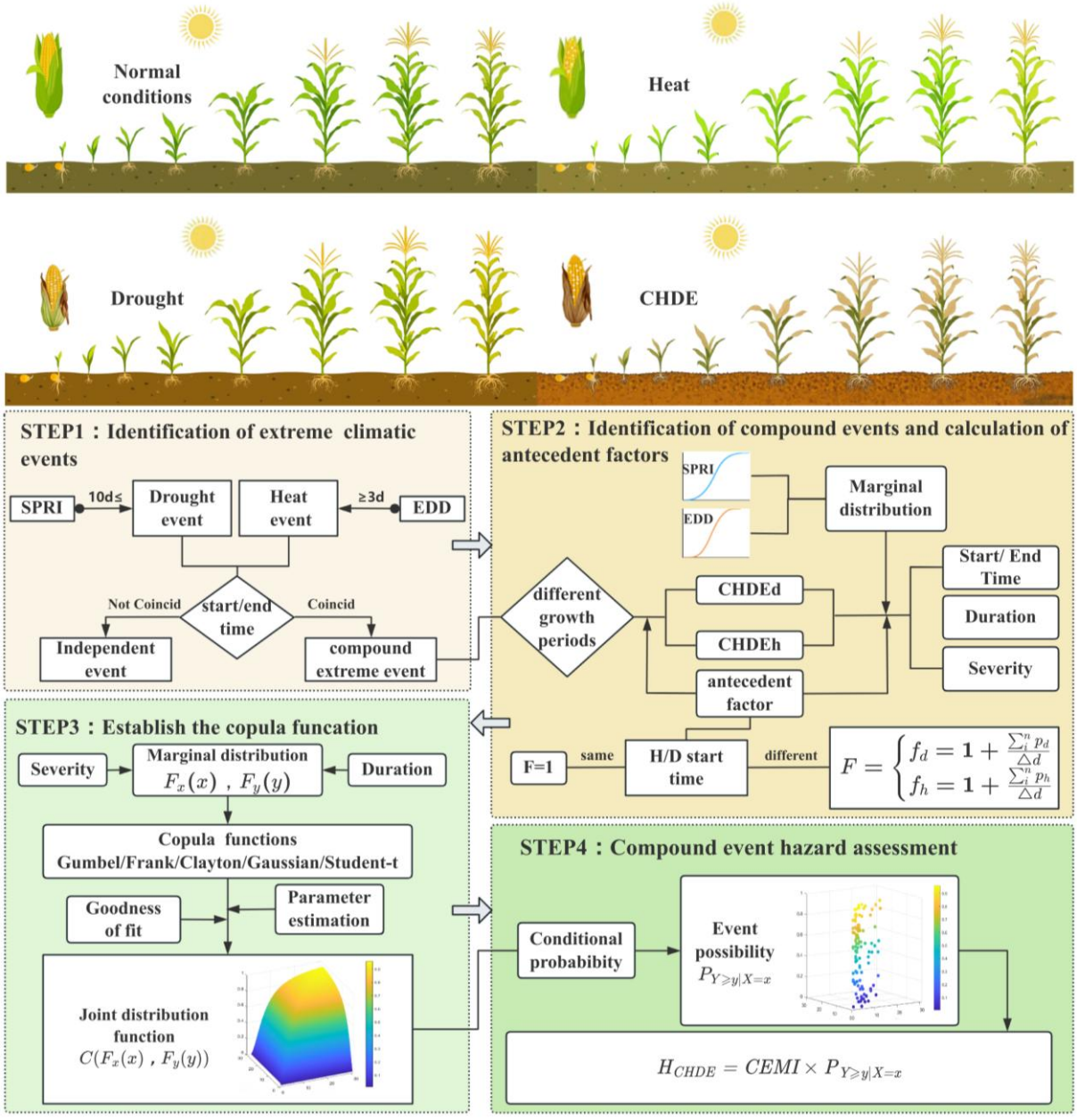

Fig 2. The methodological framework of this study.

2.3.1 Standardized precipitation requirement index (SPRI)

Previous studies have used crop coefficients for different growth stages of maize to characterize agricultural drought in the region. This index was developed by calculating water requirements across various growth stages (Chen et al. 2024; Yang et al. 2022; Li et al. 2025). Consistent with Fig 2, a drought event was defined as an uninterrupted sequence of at least 10 consecutive days with SPRI < -0.5. The event ends when SPRI ≥ -0.5, and separate sequences are not merged. The calculation process is as follows:

$$ET_0 = \frac{0.408\Delta(R_n - G) + \gamma \frac{900}{T+273} u_2 (e_s - e_a)}{\Delta + \gamma(1 + 0.34u_2)} \quad (1)$$

$$ET_c = ET_0 * K_c \quad (2)$$

where ET_0 is the potential evapotranspiration (mm); ET_c is the actual evapotranspiration (mm), and K_c is the crop coefficient, with values adopted from Wang (2012) and listed in Table 2.

$$P_{ci} = a_i * P_i \quad (3)$$

$$D_i = P_{ci} - ET_{ci} \quad (4)$$

where P_{ci} is the effective precipitation on day i (mm); P_i is the daily precipitation on day i (mm); a_i is the effective utilization coefficient, defined as follows: when $P_i \leq 5\,mm$, $a_i = 0$; when $5 < P_i \leq 50$ mm, $a_i = 0.9$; when $50 < P_i \leq 100$ mm, $a_i = 0.8$; when $P_i > 100$ mm, $a_i = 0.7$; D_i is the difference between effective precipitation and actual evapotranspiration on day i (mm).

$$f(x) = \frac{\beta}{\alpha}\left(\frac{x-\gamma}{\alpha}\right)^{\beta-1}\left(1+\left(\frac{x-\gamma}{\alpha}\right)^{\beta}\right)^{-2} \quad (5)$$

$$F_i = \frac{i-0.35}{N} \quad (6)$$

where α is the scale parameter, β is the shape parameter, and γ is the location parameter. N is the number of days included in the calculation.

$$F(x) = \left[1+\left(\frac{\alpha}{x-\gamma}\right)^{\beta}\right]^{-1} \quad (7)$$

$$SPRI = W - \frac{C_0 + C_1 W + C_2 W^2}{1 + d_1 W + d_2 W^2 + d_3 W^3} \quad (8)$$

where $p = 1 - F(x)$; when $p \leq 0.5$, $W = \sqrt{-2 \ln p}$, when $p > 0.5$, $W = \sqrt{-2 \ln (1-p)}$ and the SPRI takes the opposite value; $c_0 = 2.5155$, $c_1 = 0.8029$, $c_2 = 0.0103$, $d_1 = 1.4328$, $d_2 = 0.1893$, and $d_3 = 0.0013$.

2.3.2 Excessive degree days (EDD)

EDD is widely used to assess the impact of heat stress on crop yield (Wang et al. 2018a; Zhu et al. 2022). In this study, we used EDD to quantify heat stress intensity. A heat event was defined as at least three consecutive days with Tmax ≥ Tth. The EDD is calculated as follows:

$$EDD = \sum_{d=1}^{N} EDD_d \quad (9)$$

$$EDD_d = \begin{cases} T_{max} - T_{th} & if\ T_{max} \geq T_{th} \\ 0 & if\ T_{max} < T_{th} \end{cases} \quad (10)$$

where T_{max} is daily maximum temperature and T_{th} is the heat threshold for the corresponding maize growth stage. Following the stage-specific adverse-temperature thresholds for spring maize in Southwest China reported by Huang et al. (2017), T_{th} is set to 27, 30, 33, 35, and 30 °C for V0–VE, VE–V6, V6–R1, R1–R3, and R3–R6, respectively. The same stage-specific thresholds are applied across stations and years to maintain temporal comparability.

2.3.3 Information transformation

To combine drought and heat indices, which have different dimensions, we applied marginal distribution theory to construct the marginal distribution functions for the Drought Severity index (DS) and the Heat Degree days (HD). The intensity of heat and drought is transformed via a probabilistic approach to eliminate differences in units and magnitude. This resulted in daily non-exceedance probabilities for drought (p_d) and heat (p_h), ranging from 0 to 1. Since optimal marginal distributions for DS and HD may vary across different stations, we applied the Gringorten empirical formula to estimate the marginal distribution for each variable (DS and HD) separately, thereby mitigating uncertainty associated with the assumptions of a parametric distribution.

$$P=\frac{m-0.44}{n+0.12} \tag{11}$$

where m denotes the rank of each variable (DS in descending order and HD in ascending order), and n is the sample size.

2.3.4 Definition of the antecedent factors

Research has demonstrated that the sequence of drought and heat events is crucial in triggering CHDE. Prior exposure to drought or heat stress significantly reduces the capacity of vegetation recovery, which amplifies the adverse impacts of subsequent compound extreme events (Jing et al. 2023; Hamed et al. 2025). To better quantify the cumulative effect of preceding drought or heat stress, this study introduces two antecedent factors: (a) the drought-related antecedent factor, denoted as f_d; and (b) the heat-related antecedent factor, denoted as f_h. Their specific formulations are given as follows:

$$F=\begin{cases} f_d=1+\frac{\sum_i^n p_d}{\Delta d}, & \Delta d\geq 1 \\ f_h=1+\frac{\sum_i^n p_h}{\Delta d}, & \Delta d\geq 1 \end{cases} \tag{12}$$

where Δd represents the time difference between the start of a CHDE and the occurrence time of a drought or heat event within the same period, and p_d and p_h are the daily non-exceedance probabilities for drought and heat, respectively.

2.3.5 Definition of CHDE

CHDE occur when drought and heat events coincide temporally within the same spatial area. The composite event magnitude index (CEMI) was used to quantify CHDE severity, following the magnitude-index approach of Wang et al. (2021). For each event, daily compound intensity was represented by the product of the drought and heat non-exceedance probabilities defined in Section 2.3.3. These daily values were accumulated over all overlapping drought and heat days and then multiplied by

the event-specific antecedent factor defined in Section 2.3.4. Event severity was calculated as follows:

$$CEMI = F \sum_{i=1}^{D} \left(P_{d,i} \times P_{h,i}\right) \quad (13)$$

where CEMI represents the severity of an individual CHDE, D is the number of overlapping drought and heat days within the event, $P_{d,i}$ and $P_{h,i}$ are the drought and heat non-exceedance probabilities on overlapping day i, respectively, and F is the antecedent factor associated with that event.

2.3.6 Calculating the probability of CHDE occurrence

The copula function is a multivariate joint distribution function defined based on uniform marginal distributions on the interval [0,1]. Its construction was independent of the marginal distributions of the variables (Wu et al. 2020; Zhang et al. 2022b). The introduction of copula provides a powerful tool for modeling the multivariate features of compound events. Copula modeling typically involves three key steps: (1) selection of marginal distributions; (2) selection of a copula function family; and (3) validation of the copula model. In this study, suitable marginal distributions were selected from five common univariate distributions (Normal, Lognormal, Gamma, Generalized Extreme Value, and Weibull), and the goodness-of-fit was evaluated using the nonparametric Kolmogorov-Smirnov (K-S) test. Joint distribution models were constructed based on five classical copula functions (Frank, Gumbel-Hougaard, Clayton, Gaussian, and Student-t copula). The Akaike Information Criterion (AIC) was used as the primary model-selection criterion, and root mean square error (RMSE) was used as a diagnostic of agreement between empirical and theoretical joint probabilities.

$$RMSE=\sqrt{\frac{1}{n}\sum_{i=1}^{n}(p_i-p_{ei})^2} \quad (14)$$

$$AIC = -2\sum_{i=1}^{n} lnc_{\theta}(u_i, v_i) + 2k \quad (15)$$

where n is the sample size, p_i and p_{ei} are the theoretical and empirical joint probabilities, respectively, and $c_{\theta}(u_i, v_i)$ is the copula density evaluated at the observations transformed using the fitted marginal distributions. AIC is calculated from the copula log-likelihood with the marginal fits held fixed across candidate copulas. The number of free copula parameters is $k = 1$ for the bivariate Gaussian, Frank, Clayton, and Gumbel copulas and $k = 2$ for the bivariate Student-t copula. Lower *AIC* indicates a better balance between model fit and complexity, whereas lower *RMSE* indicates closer agreement with empirical probabilities.

For a CHDE with a given severity (CEMI), its duration is variable, and the corresponding occurrence probability depends on the specific duration. This probability can be derived from a conditional

distribution. According to copula theory, for a pair of continuous random variables, X (duration) and Y (severity), with X fixed at a specific value x, the conditional probability is given by:

$$F_{Y|X(y|x)}=P(Y\geq y|X=x)=1-\frac{\partial F(x,y)/\partial x}{dF_X(x)/dx}=1-\frac{\partial C(u,v)}{\partial u} \quad (16)$$

where x and y denote the duration and severity of the CHDE, respectively. $F_X(x)$ and $F_Y(y)$ represent the marginal distributions of duration and severity, taking values in [0,1]. $C(u,v)$ is the optimal copula function.

2.3.7 Hazard assessment

CHDE hazard was quantified by combining event magnitude with the conditional probability associated with event duration and severity. Events with greater magnitude and higher conditional occurrence probability therefore received larger hazard values.

$$H=CEMI\times P_{(Y\geq y,\ X=x)} \quad (17)$$

where H is the dimensionless CHDE hazard index, $CEMI$ is combined-event magnitude, X is event duration, Y is event severity, and $P_{(Y\geq y,\ X=x)}$ is the fitted conditional exceedance probability of severity given duration. The index supports relative comparison among stations, growth stages, and periods.

2.3.8 Wavelet analysis

Wavelet analysis was used to examine the temporal variability of the annual CHDE hazard series across maize growth stages during 1961–2023. By translating and dilating a mother wavelet, the method decomposes a time series at multiple scales and describes how oscillatory patterns vary over time (Zhang et al. 2022a; Qu et al. 2024). The continuous wavelet transform of a time series $f(t)$ is defined as:

$$W_f(a,b)=\frac{1}{\sqrt{a}}\int_{-\infty}^{+\infty} f(t)\varphi^*\left(\frac{t-b}{a}\right)dt \quad (18)$$

where $W_f(a,b)$ denotes the wavelet coefficient, a is the scale parameter, b is the temporal translation parameter, φ is the mother wavelet, and the superscript * denotes complex conjugation.

The wavelet variance reflects the distribution of signal energy across temporal scales. It helps identify the dominant periodicities of a time series and assess the relative strength of fluctuations at different scales. The wavelet variance is calculated as follows:

$$W_p(a)=\int_{-\infty}^{+\infty}\left|W_f(a,b)\right|^2 db \quad (19)$$

where $W_p(a)$ denotes the wavelet variance at scale a, $W_f(a,b)$ is the wavelet coefficient at scale a and temporal position b, and $\left|W_f(a,b)\right|^2$ represents the wavelet power.

3. Results

3.1 Drought and heat exposure across growth stages

Fig 3 shows the spatial distribution of drought and heat event frequency across the growth stages of spring maize during 1961–2023, providing a basis for examining the antecedent conditions of CHDE. The results indicate that drought events occurred mainly during VE–V6, V6–R1, R1–R3, and R3–R6. V6–R1 had the highest drought frequency, with 25–56 events during 1961–2023. During VE–V6 and V6–R1, drought frequency was relatively high in the western and southwestern parts of the study area, particularly in Zone IV. Spatial differences were less pronounced during R1–R3. During R3–R6, the spatial pattern reversed, with higher drought frequency in the east and lower frequency in the west. Heat events occurred most frequently during VE–V6 and R3–R6. Zone I was a high-frequency area during VE–V6, while heat events were widespread across the study area during R3–R6, with 117–167 events over the full record.

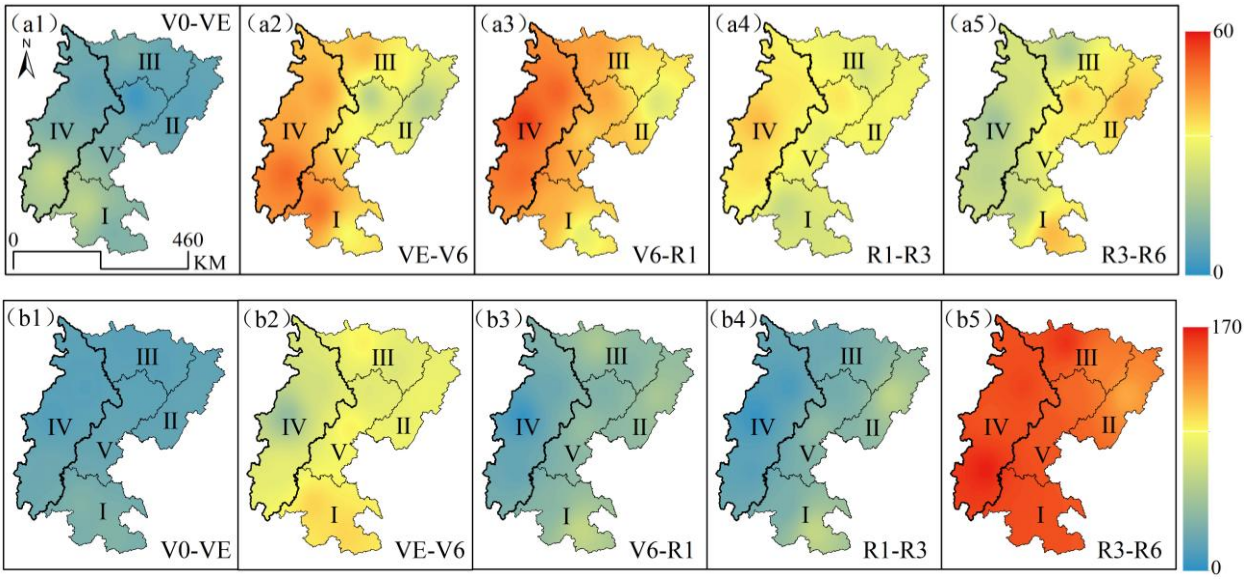

Fig 3. Spatial distribution of drought event frequency (a1–a5) and heat event frequency (b1–b5) during different growth stages of maize.

Fig 4 shows the ratio of drought days and heat days to the total number of days in each growth stage of spring maize in the CSC Hills from 1961 to 2023. The results indicate clear differences in exposure to drought and heat across growth stages. During V0–VE, VE–V6, V6–R1, and R1–R3, the proportion of drought days was higher than that of heat days. In contrast, during R3–R6, the proportion of heat days exceeded that of drought days. However, the proportion of drought days during this stage remained considerable and increased markedly after 2000, particularly during 2017–2023.

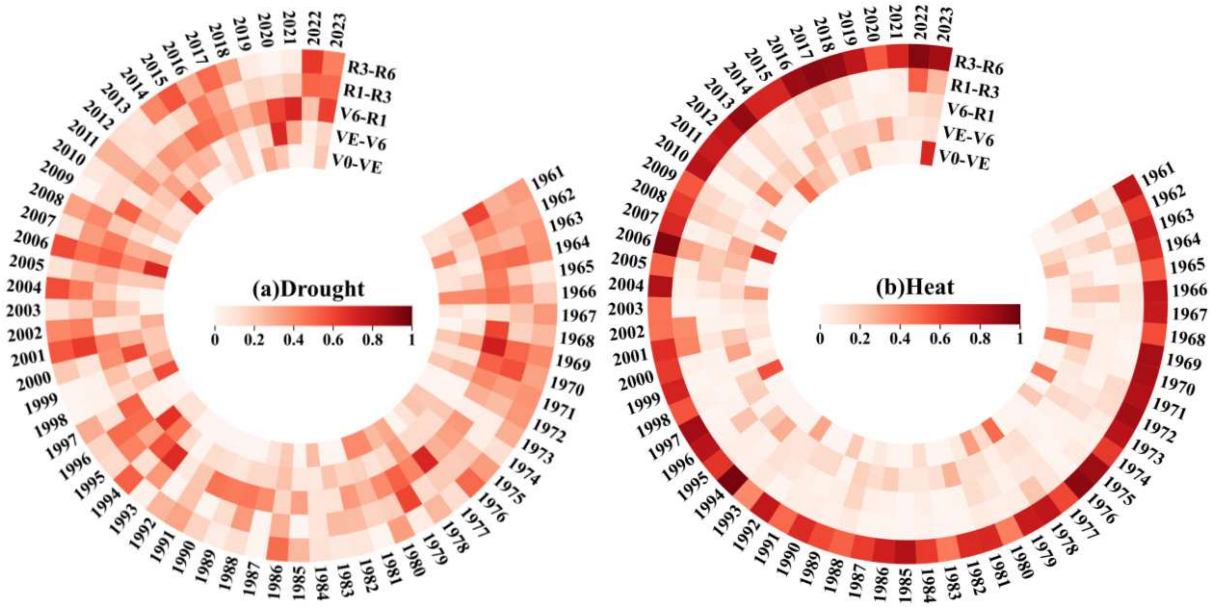

Fig 4. Annual proportion of drought days (a) and heat days (b) relative to the total number of days in each growth stage.

3.2 Characteristics of antecedent factors

Fig 5 shows the spatial distributions of time-averaged antecedent factors (with zero values included in the averaging) across spring maize growth stages, with drought-related factors predominating. The drought-related antecedent factors (a1–a5) were relatively low during V0–VE, increased during VE–V6, and showed a northern high-value area during V6–R1, with values exceeding 0.6 in some locations. They weakened during R1–R3 and increased again during R3–R6, when an extensive high-value area occurred in the east and north. In contrast, the heat-related antecedent factors (b1–b5) were weaker overall. Moderately high values appeared only in the southern, eastern, and northern regions during the R3–R6 stage.

The proportional analysis (Fig 5c) further confirmed the dominance of drought-related antecedent factors. Their proportion remained above 0.69 throughout the growing season and reached 1 during V0–VE. From VE–V6 to R1–R3, the drought-related proportion remained between 0.82 and 0.90, whereas the heat-related proportion remained comparatively low. From 1961–1992 to 1993–2023, the heat-related proportion decreased from 0.239 to 0.149 during VE–V6 but increased from 0.098 to 0.133 during R1–R3. During R3–R6, drought- and heat-related proportions were approximately 0.7 and 0.3, respectively, indicating that drought remained dominant while the relative contribution of heat was highest at this stage.

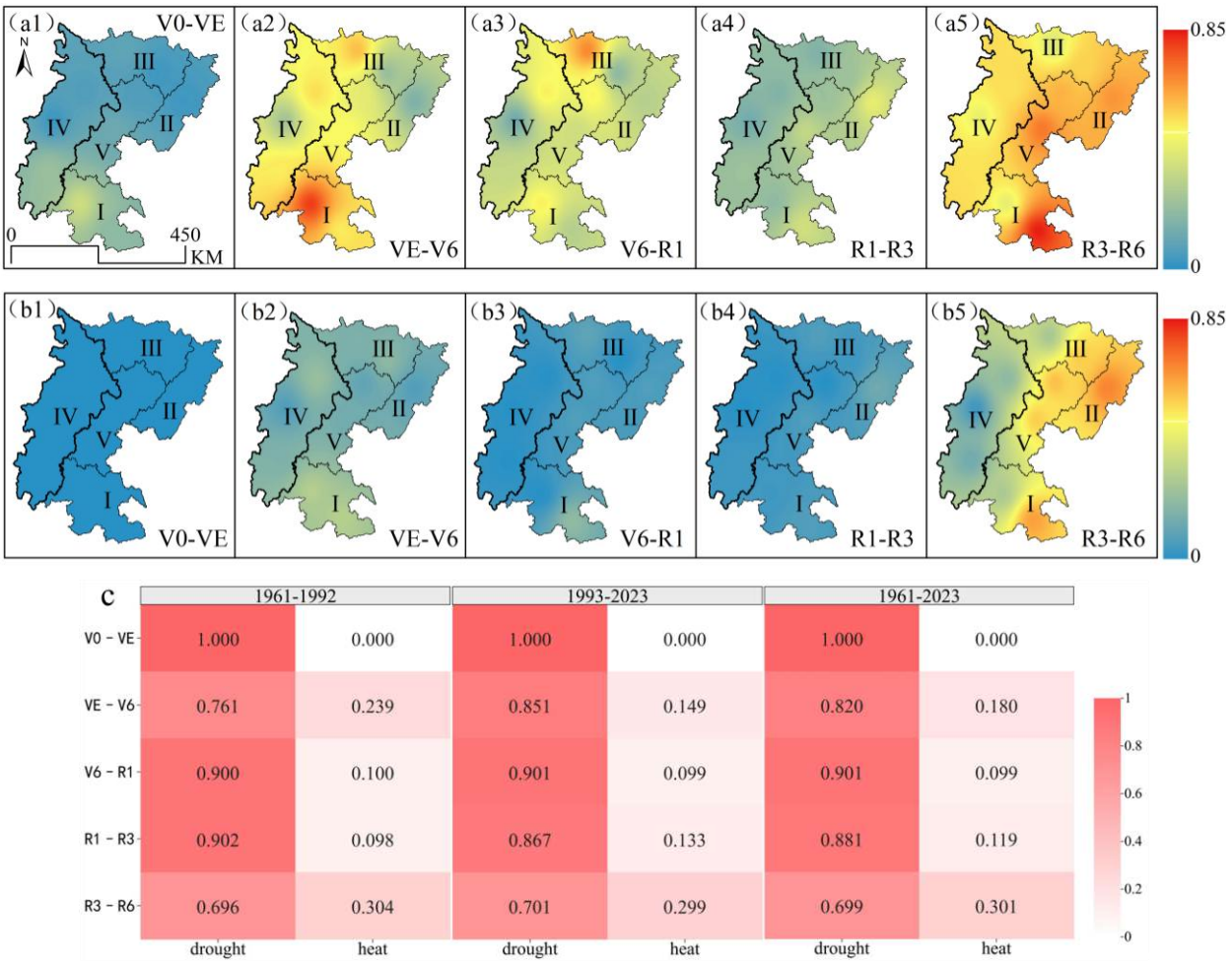

Fig 5. Spatial distributions of time-averaged antecedent factors (with zero values included in the averaging) associated with drought (a1–a5) and heat (b1–b5) across different growth stages, and their proportion (c).

Fig 6 further presents the annual variations in spatially averaged drought-related and heat-related antecedent factors across spring maize growth stages during 1961–2023. Overall, the values of drought-related antecedent factors were also generally higher than those of heat-related antecedent factors. Drought-related antecedent factors exceeded 1.5 during VE–V6 and R3–R6, reaching a maximum of 1.71 during R3–R6 in 2001. Heat-related antecedent factors were most prominent during R3–R6 and reached 1.32 in 2015. Drought-related antecedent factors were more frequently elevated after 2000, whereas heat-related antecedent factors showed no clear monotonic pattern. Together, Figs 5–6 show that drought-related antecedent factors predominated across growth stages, while heat-related antecedent factors were most prominent during R3–R6.

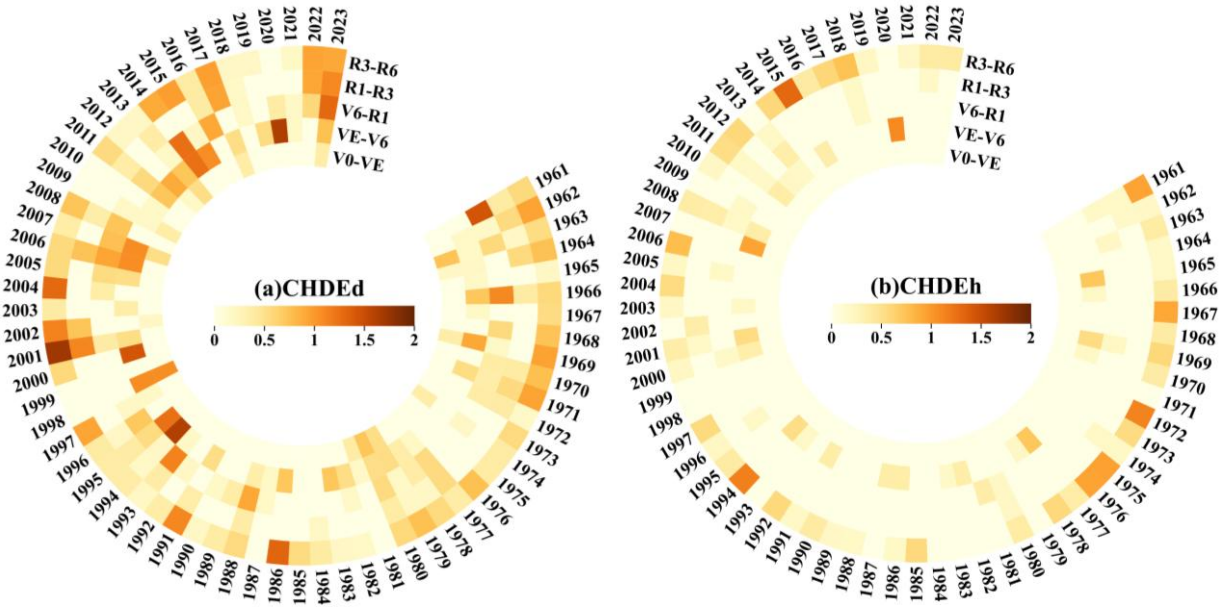

Fig 6. Annual variations in spatially averaged antecedent factors associated with drought (a) and heat (b) across spring maize growth stages.

3.3 Spatiotemporal evolution of CHDE

Previous studies have shown that the climate system of China, especially in the southwestern region, underwent a significant shift around the 1990s. This shift included increases in the frequency, duration, severity, and spatial extent of CHDE (Yu and Zhai 2020; Pan et al. 2024; Wang et al. 2024). Against this background, the study period (1961–2023) was divided into two approximately equal sub-periods, 1961–1992 (32 years) and 1993–2023 (31 years), to compare CHDE characteristics and hazard over time.

3.3.1 Spatiotemporal characteristics of CHDE frequency and duration

Fig 7 illustrates the spatial distribution of CHDE frequency across different growth stages during 1961–1992 and 1993–2023. Overall, VE–V6, V6–R1, and R3–R6 were the primary stages with frequent occurrence of CHDE. In these stages, CHDE frequency over 1961–2023 generally ranged from 10 to 50 events (combined counts for the two periods) and exceeded 60 events (combined counts for the two periods) in some local areas. A comparison of the two periods reveals a clear increase in CHDE frequency. The spatial pattern evolved from scattered high-value areas to broader regional coverage. During 1961–1992, high-frequency areas (14–30 events) were mainly distributed in the eastern and northeastern parts of the study area, showing a general pattern of gradual decrease from east to west. During 1993–2023, CHDE intensified and expanded toward the western and southern regions in most growth stages. Zone I was identified as a high-frequency area. CHDE frequency showed a marked increase in Zones II and III.

Zone IV remained at a relatively low level but showed a consistent upward trend compared with the earlier period. Among all stages, VE–V6 exhibited the largest increase in CHDE frequency. Additionally, R3–R6 showed a distinct spatiotemporal heterogeneity. CHDE intensified in the western part of the study area but weakened in the eastern part, particularly in Zones II, III, and V.

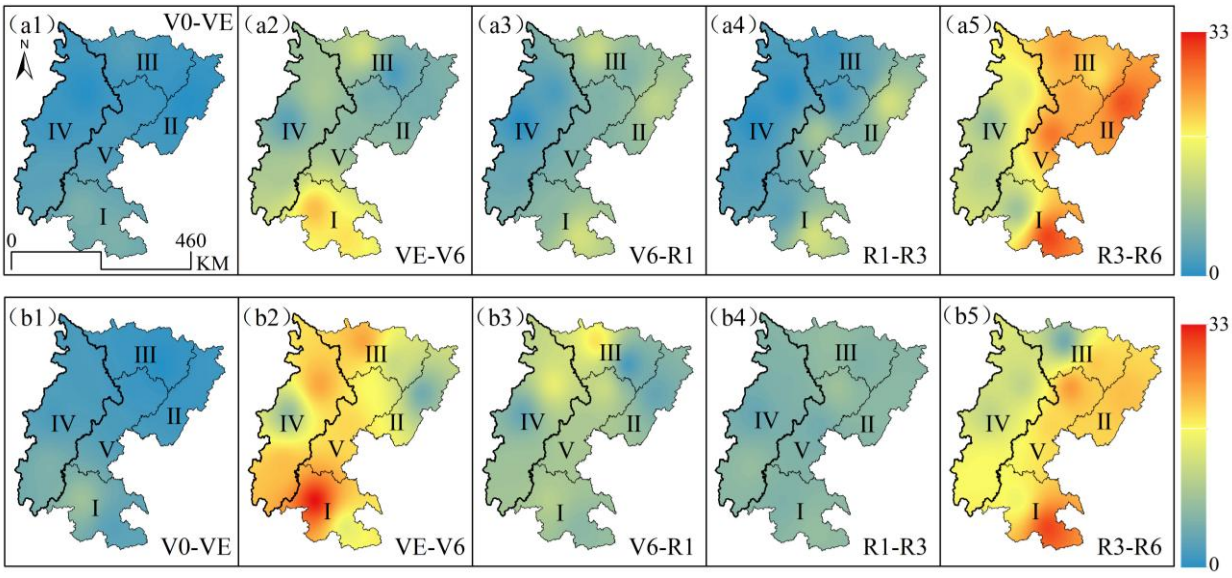

Fig 7. Spatial distribution of CHDE frequency during the two periods (1961–1992: a1–a5; 1993–2023: b1–b5).

Based on the spatial distribution maps and violin plot of CHDE duration for 1961–1992 and 1993–2023 (Fig 8), the spatiotemporal characteristics of CHDE duration across growth stages are summarized as follows. R3–R6 consistently exhibited the longest CHDE duration. During 1961–1992, the median duration was generally 7–10 days, which was substantially higher than in other stages. During 1993–2023, the median increased to 9–14 days across the region. In some areas, extreme events exceeded 30 days. This stage, therefore, represents the most sensitive and high-hazard period in the maize growth cycle. Clear spatial differences were observed in both periods. Zones II and III repeatedly exhibited long CHDE duration during several stages, including V6–R1, R1–R3, and R3–R6. After 1993, this high-duration area expanded. From a temporal perspective, high-duration areas covered a much larger region during 1993–2023 than during 1961–1992. The overall statistical distribution of CHDE duration also showed a pronounced upward shift after 1993. In most stages, the median duration increased, and the interquartile range widened. This pattern indicates not only a longer average duration but also a higher frequency of extreme long-duration events (>20 days). The increasing trend was most prominent in the R3–R6 stage. During 1993–2023, the mean CHDE duration at most locations was approximately 1–3 days longer than during 1961–1992.

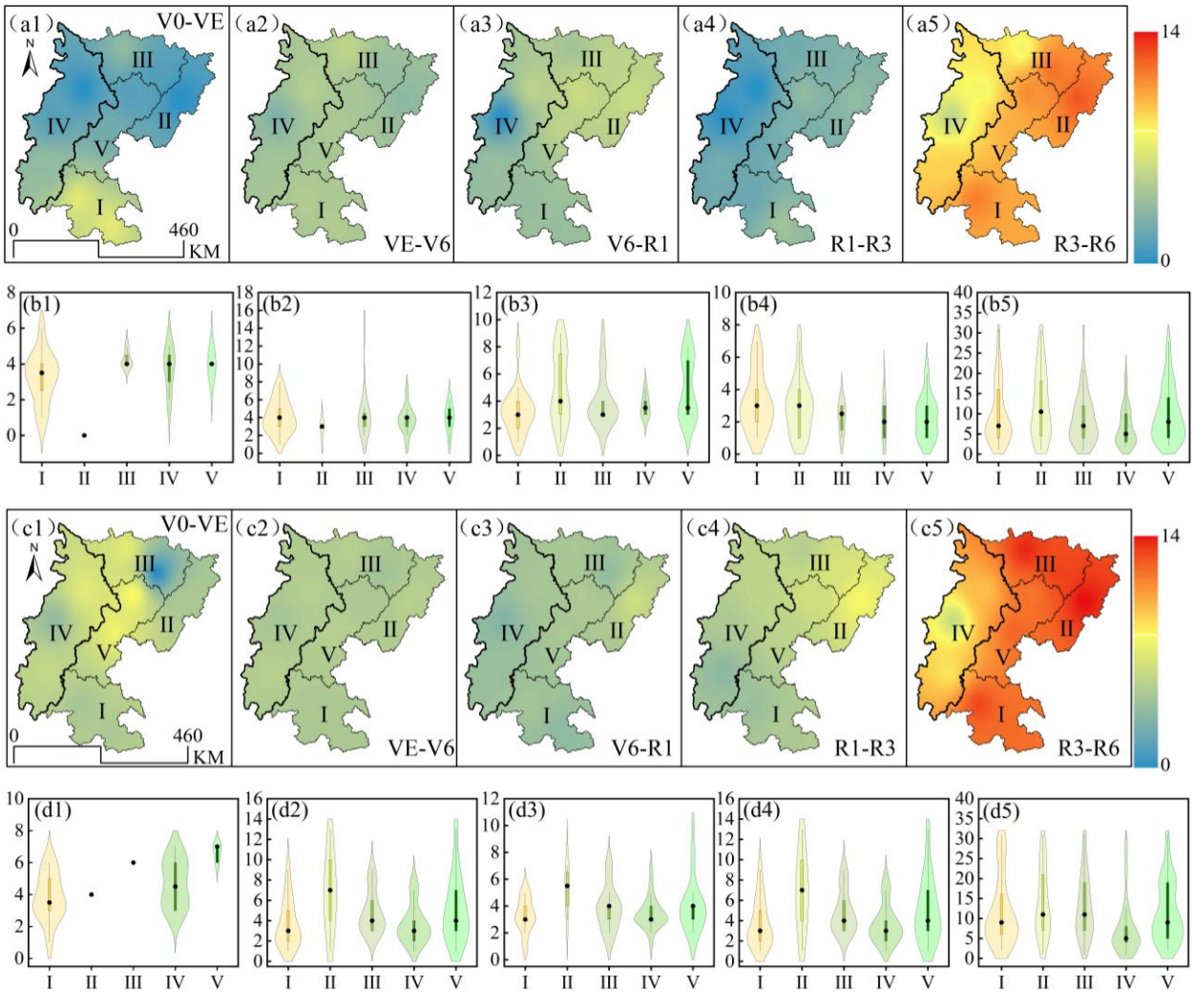

Fig 8. Spatial distribution of CHDE duration during the two periods (1961–1992: a1–b5; 1993–2023: c1–d5).

3.3.2 Spatiotemporal characteristics of CHDE severity

Fig 9 shows the spatial distributions and violin plots of CHDE severity for the two periods. CHDE severity exhibited pronounced spatiotemporal variation, and R3–R6 was the most critical stage. Its mean severity index consistently exceeded 10, substantially higher than at other growth stages.

During 1961–1992, CHDE severity was relatively low across most growth stages. From V0–VE to R1–R3, the indices of both median and mean severity were generally below 6. Spatial differences were limited during these stages. Areas with relatively higher severity were mainly located in the northern and northeastern parts of the study area. The overall pattern showed lower values in the southwest and higher values in the northeast. However, these high-severity areas were geographically restricted. A clear shift occurred during R3–R6, where CHDE severity increased markedly and exceeded 10 in many areas. Regional differences also became more pronounced. In the eastern parts of Zones II and III, the median

severity exceeded 10, and the mean value rose above 15. These values were substantially higher than those in other regions.

In contrast, the period 1993–2023 exhibits a clear overall increase in CHDE severity. Spatially, severity during V0–VE and VE–V6 increased only slightly compared with 1961–1992. However, during V6–R1 and R1–R3, the core high-severity area shifted from the northern part of the region toward the southeast. The high-severity area also expanded. The largest increase occurred during R3–R6, where the mean severity increased by approximately 3 to 5 units across the region. In Zones II and III, the mean severity reached 20.5 and 23, respectively. The violin plots show a wider distribution of severity values during R3–R6 in the later period. This pattern indicates stronger interannual variability and more frequent high-severity CHDE.

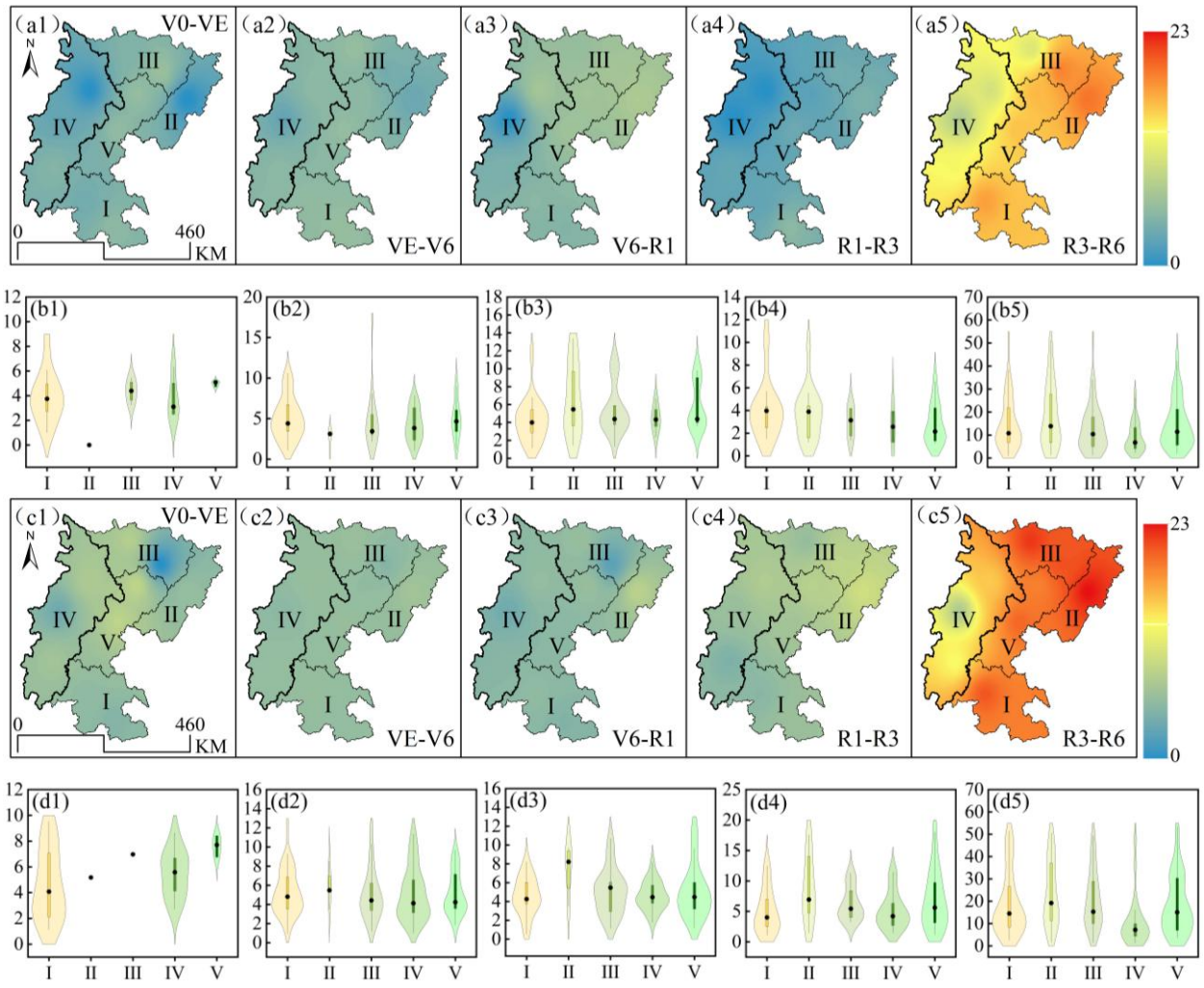

Fig 9. Spatial distribution of CHDE severity during the two periods (1961–1992: a1–b5; 1993–2023: c1–d5).

3.4 Hazard assessment of CHDE

3.4.1 Copula functions and joint probability distribution

Five copula functions (Gumbel-Hougaard, Frank, Clayton, Gaussian, and Student-t) were fitted to CHDE duration–severity pairs for 1961–2023. The goodness-of-fit results are summarized in Table 3. The Student-t copula yielded the lowest AIC (-3269.07), whereas the Gaussian copula yielded the lowest RMSE (0.0534). Because AIC was the primary selection criterion and the Student-t RMSE (0.0576) remained comparable to those of the other models, the Student-t copula was selected to represent the dependence between CHDE duration and severity. The fitted joint distribution is shown in Fig 10a.

Table 3. Goodness-of-fit evaluation for the joint probability distribution of CHDE severity and duration for spring maize.

Copula	AIC	RMSE
Gumbel-Hougaard	-3257.79	0.0562
Frank	-2312.3	0.0666
Clayton	-2955.19	0.0538
Gaussian	-2976.19	0.0534
Student-t	-3269.07	0.0576

Short-duration CHDE had the highest conditional occurrence probabilities in the study region. Probabilities of 0.8–0.9 generally corresponded to events lasting 0–10 days and decreased sharply with increasing duration. For durations of 20–30 days, only low- to moderate-severity events retained probabilities of 0.4–0.6. When duration exceeded 30 days and severity was above 20, probability generally fell below 0.2.

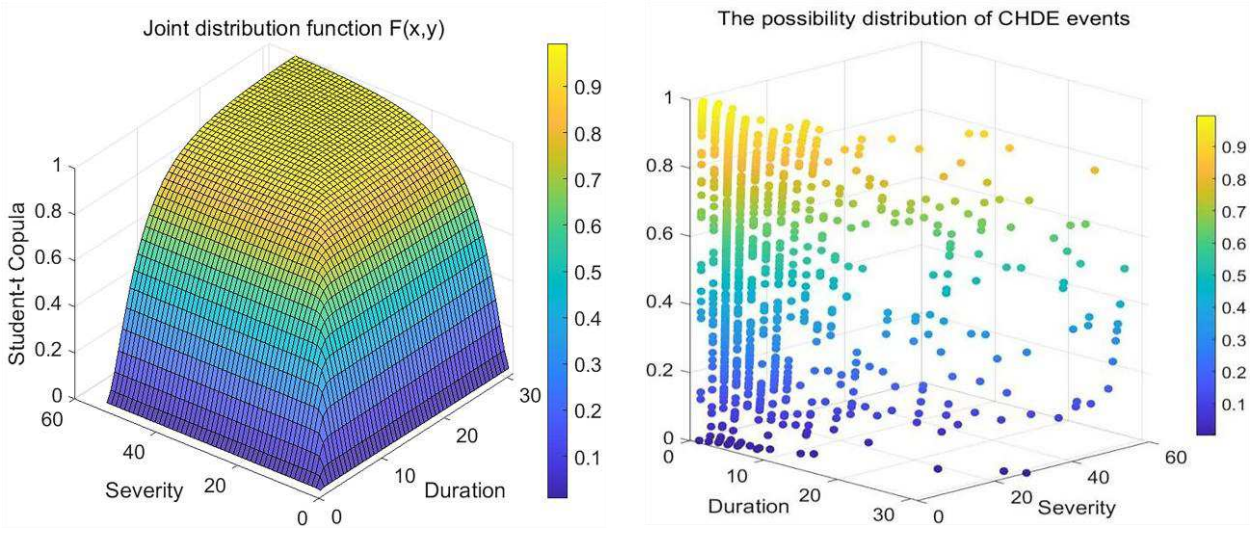

Fig 10. (a) Two-dimensional copula joint distribution; (b) Probability distribution of CHDE occurrence across different durations and severity levels.

3.4.2 Spatiotemporal patterns of CHDE hazard

The hazard assessment identified R3–R6 as the stage with the highest CHDE hazard in the CSC Hills (Fig 11). During 1961–1992, hazard values from V0–VE through R1–R3 were generally below 0.55. By contrast, values during R3–R6 exceeded 2 in most areas and were generally above 7 in the eastern region. The spatial pattern during 1993–2023 was broadly similar, with low hazard at most earlier growth stages and persistently high hazard during R3–R6. Hazard increased most clearly during VE–V6 and R3–R6. During R3–R6, the mean hazard index was approximately 1.4 higher than during 1961–1992, with increases above 4 in southern Zone I and northern Zone V. Spatial differentiation during R3–R6 retained an east-high, west-low pattern.

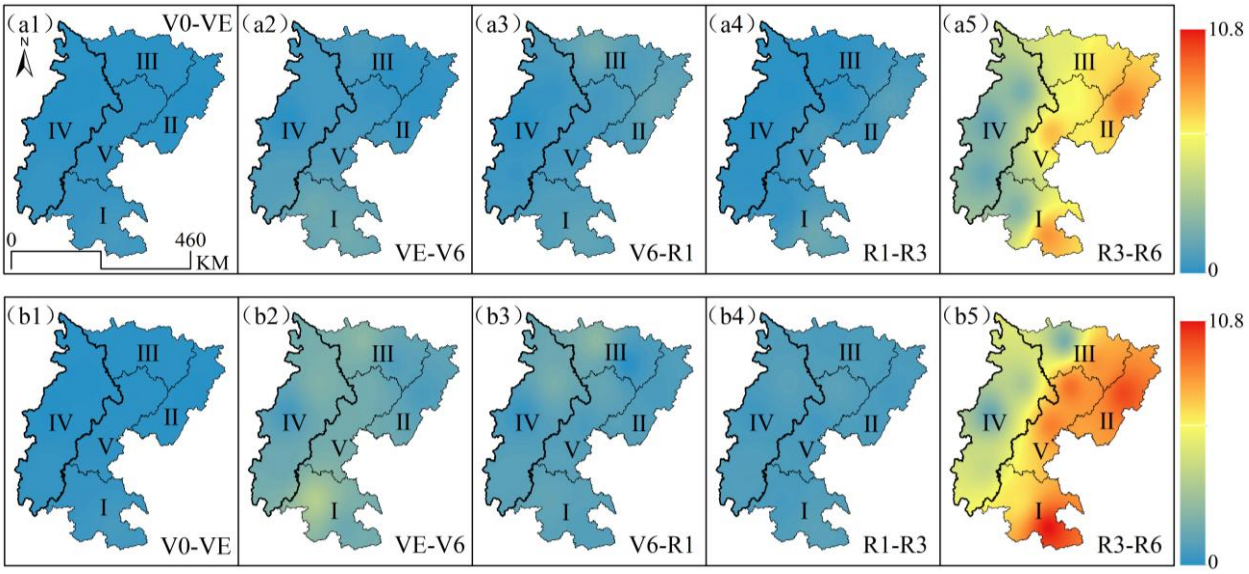

Fig 11. Spatial distribution of CHDE hazard during the two periods (1961–1992: a1–a5; 1993–2023: b1–b5).

The wavelet time-frequency spectrum (Fig 12) reveals the fluctuation intensity of CHDE hazard across growth stages at the annual scale. For VE–V6, V6–R1, R1–R3, and R3–R6, fluctuations were relatively weak during 1961–1980 across most scales. After 1980, fluctuation amplitude increased with both time and scale. After 2000, clusters of high amplitude appeared at medium-to-high scales (>20). This pattern indicates stronger fluctuations in recent decades and a gradual shift of the dominant variability toward longer periodic cycles. It suggests that the system has become increasingly sensitive to interdecadal climate variability over time. V0–VE exhibits a different pattern. After 2020, high-amplitude signals were mainly concentrated at medium scales (25–30). Overall intensity remained low, and the range of scales was limited. This result suggests that the seedling stage responds primarily to medium-period climate fluctuations in recent years. The wavelet variance plots (Fig 12, right panels) further identify the dominant cycles. For VE–V6, R1–R3, and R3–R6, variance increases steadily with

scale and shows no clear peak. This pattern indicates that variability is mainly controlled by long interdecadal cycles (>30 years) and reflects sensitivity to long-term cumulative climate effects. In contrast, V0–VE and V6–R1 exhibit distinct variance peaks at scales of 25–30 years, corresponding to cycles of approximately 26–31 years. This finding indicates that variability in these stages is primarily driven by climate oscillations with medium interdecadal periods and shows clear scale dependence.

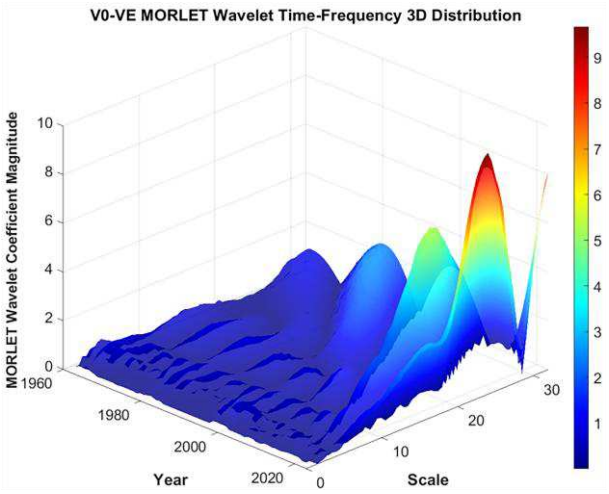

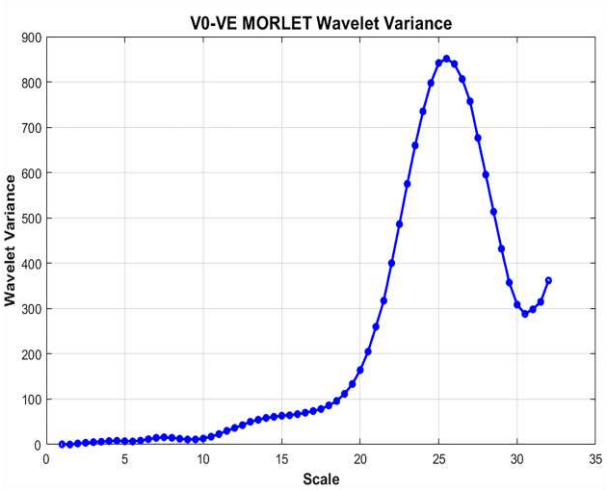

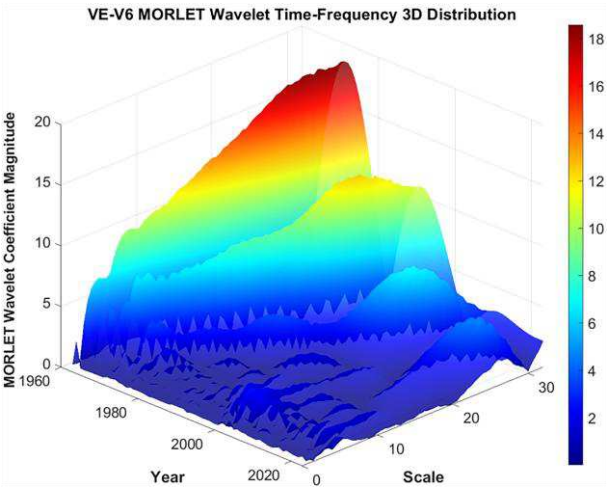

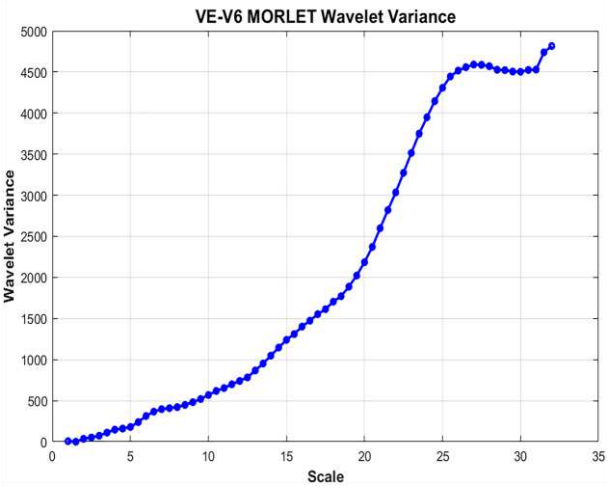

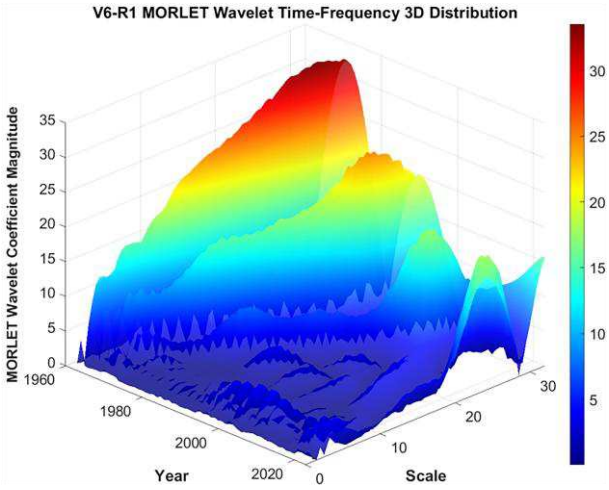

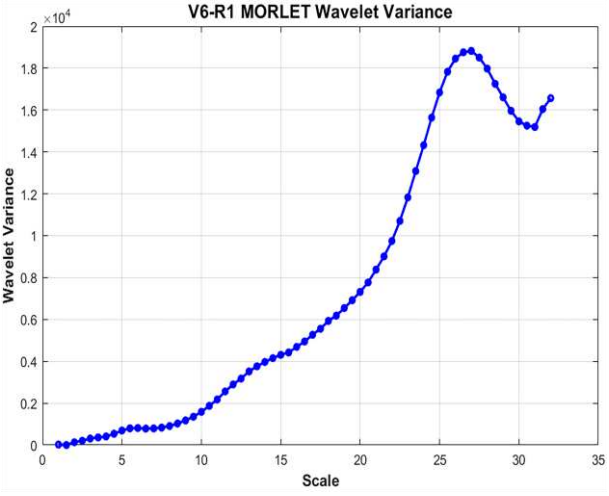

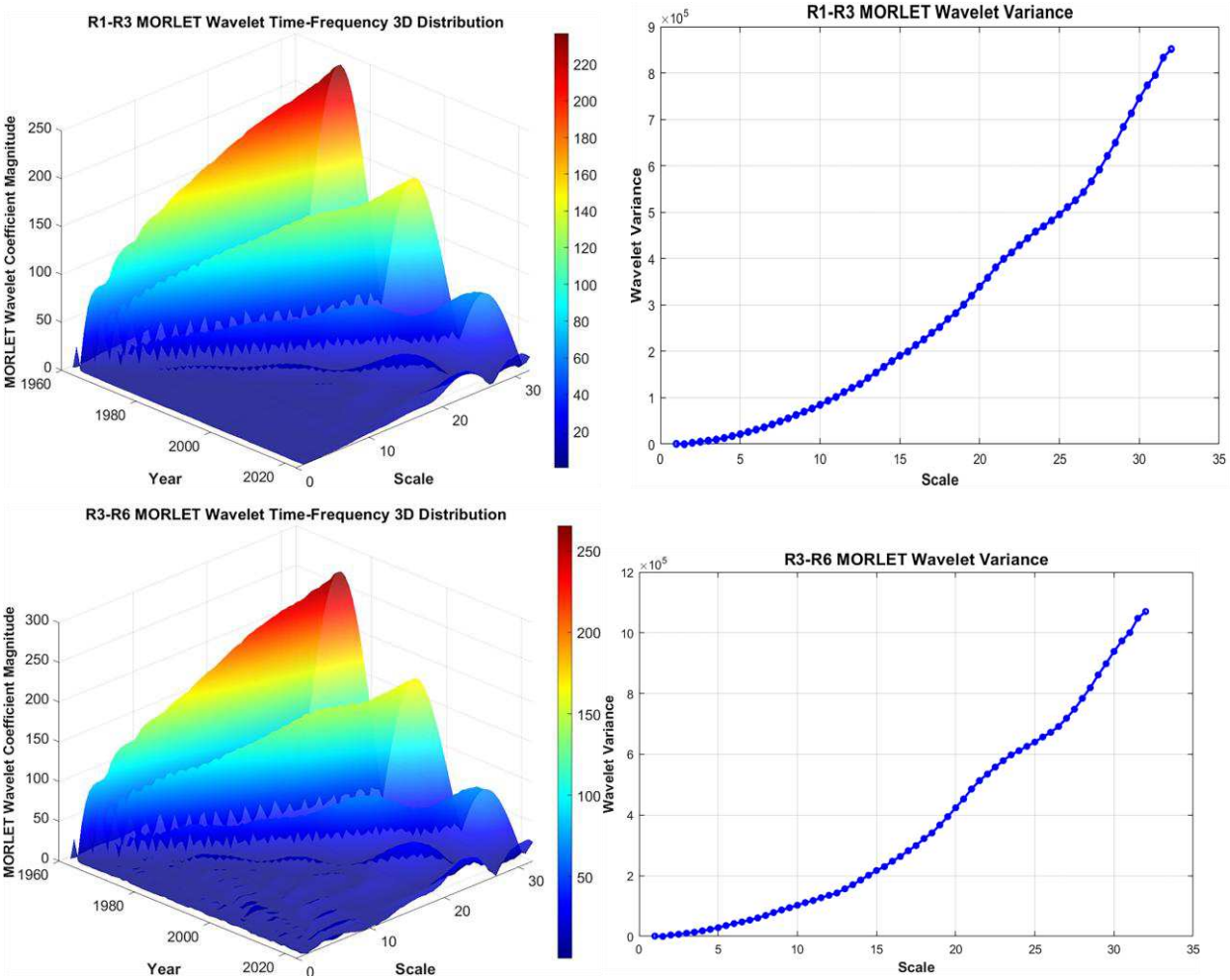

Fig 12. Three-dimensional wavelet time–frequency spectrum (real part) and wavelet variance for different growth stages.

4. Discussion

4.1 Stage-specific differences in drought, heat, and antecedent stress

This study revealed clear spatiotemporal heterogeneity in drought and heat events across the growth stages of spring maize in the CSC Hills. It also identified differences in their dominant antecedent factors. Drought events exhibited higher exposure and stronger antecedent contributions than heat events in most growth stages, particularly during VE–V6 and V6–R1 (Figs. 3a2, a3). Drought also intensified over the growing season. This finding was consistent with reports of increasing drought frequency in southwestern China, particularly in late spring and early summer (Zhao et al. 2024; Wang et al. 2023d). These changes reflect shifts in the regional water cycle. From V0 to R3, the proportion of drought days generally exceeded that of heat days (Fig 4). This pattern indicated that water stress was the primary and persistent environmental factor affecting crop growth. Heat events and their antecedent effects exhibited pronounced differences across growth stages. VE–V6 and R3–R6 were the main high-incidence periods (Figs. 3, 4).

Although regional warming has continued and many studies have reported an overall increase in extreme heat events (Xue et al. 2020; Kuang et al. 2024), heat events defined by fixed absolute thresholds showed pronounced interannual variability without a clear upward pattern (Fig 4). The high incidence during VE–V6 may be related to the relatively low heat tolerance threshold (30 °C) at this stage. The lack of a clear upward pattern may reflect the fact that, under pronounced interannual variability in the monsoon climate, daily maximum temperatures have not yet systematically exceeded this fixed threshold. In contrast, the intensification of drought agrees with previous studies that reported decreasing precipitation (Song et al. 2024).

Heat further aggravated drought through synergistic effects (Song et al. 2024). Higher temperatures raised land surface temperature and accelerated soil moisture loss. As a result, agricultural drought became more severe. These processes strengthened the connection between meteorological drought and agricultural drought (Wei et al. 2024; Qian et al. 2024; Xiao et al. 2024). From the perspective of hydrological processes and memory effects, drought-related antecedent factors form a persistent "water stress memory" throughout the whole growth period, directly limiting the physiological regulation and plant growth and development. In contrast, heat-related antecedent factors were mainly concentrated in R3–R6 (Figs. 5, 6). Therefore, compound drought–heat stress in this region did not result from anomalies in a single meteorological variable. It developed through the interaction between reduced soil moisture and elevated temperature. Low soil moisture increased surface heating, and higher temperatures further dried the soil. This feedback intensified stress and highlights the complex interactions among climate, hydrology, and crop growth.

4.2 Stage-specific differences in CHDE characteristics and hazard

This study revealed clear stage-specific and spatiotemporal variation in CHDE characteristics and hazard. The eastern part of the study area formed the principal high-hazard region. CHDE frequency, duration, severity, and hazard generally increased over time, consistent with previous studies (Liang et al. 2025; Zheng et al. 2025). Within the growing season, V6–R6 was the critical period for CHDE hazard, with R3–R6 being particularly prominent. CHDE duration, severity, and the integrated hazard index were highest during R3–R6, and this stage exhibited the largest increases in all characteristics except frequency.

CHDE frequency declined during R3–R6 in the eastern part of the study area (Zones I, II, III, and V), while mean event duration increased by approximately 1–3 days. Longer continuous events can reduce

the number of separate events while increasing the magnitude of each event. Accordingly, although long-duration, high-severity events had lower conditional occurrence probabilities, their hazard values increased markedly because the hazard index also incorporated event magnitude.

The stage-specific evolution of CHDE reflected the seasonal concurrence of water deficit and high temperature. Previous studies reported that rising temperature has contributed substantially to CHDE evolution in China and can intensify event severity (Shi et al. 2024; Xiang et al. 2024). In this study, the consistently high heat-event frequency and CHDE hazard observed during VE–V6 and R3–R6 indicated that heat events were the key contributors to CHDE hazard affecting maize. Drought-related antecedent stress nevertheless remained dominant across all growth stages, indicating that the relative roles of drought and heat differed between antecedent stress and event-stage hazard.

4.3 Implications for maize management

CHDE management should account for both growth-stage differences in event characteristics and the sensitivity of maize yield formation. During VE–V6, CHDE occurred frequently and exhibited the largest increase in frequency between the two periods (Fig 7), supporting earlier monitoring of water deficits and heat exposure. Rainfall and temperature forecasts could be combined with soil-moisture observations to prepare for approaching compound events. Frequent CHDE during V6–R1 also deserve attention as maize approaches tasseling and silking, when combined drought and heat stress can cause substantial yield losses (Hu et al. 2023; Meena et al. 2024). During R1–R3, the expansion of high-severity areas in 1993–2023 further emphasizes the importance of protecting early grain filling from compound stress (Fig 9). Management during these reproductive stages should coordinate timely supplemental irrigation with heat warnings and, where feasible, canopy-temperature monitoring.

During R3–R6, CHDE had the longest duration, greatest severity, and highest hazard, with pronounced increases during the later period (Figs. 8–11). These findings support sustained drought–heat monitoring throughout the remaining grain-filling period, particularly in the eastern high-hazard region. Irrigation scheduling should consider soil-water availability, remaining crop water requirements, and the expected persistence of high temperatures. Field experiments have shown that supplemental irrigation can reduce maize canopy temperature and mitigate heat-related yield losses (Jian et al. 2024), providing a basis for coordinating water-deficit relief and canopy heat-stress management. Longer-term adaptation could also combine locally tested drought- and heat-tolerant cultivars with sowing dates evaluated against regional rainfall and temperature patterns. Field research in a subtropical monsoon region highlights the

511 importance of sowing-date selection for maize heat exposure and yield formation (Cao et al. 2024).

512 These stage-specific measures should also incorporate conditions preceding CHDE. Drought-related
513 antecedent factors predominated across growth stages, while the relative contribution of heat-related
514 antecedent factors was greatest during R3–R6 (Figs. 5–6). This pattern supports advance soil-water
515 conservation and irrigation planning alongside monitoring of preceding heat exposure. Combining
516 antecedent conditions with crop water requirements and rainfall and temperature forecasts could help
517 identify developing water deficits likely to coincide with subsequent heat events. Such information would
518 guide earlier management and the allocation of resources across sensitive reproductive stages and
519 prolonged compound events later in the growing season.

520 **4.4 Limitations**

521 Although this study advanced the assessment of spring maize CHDE hazard in the hilly region of
522 Southwest China, two limitations should be considered. First, the hazard framework represented the
523 influence of antecedent drought and heat stress using the cumulative mean of non-exceedance
524 probabilities within the interval between antecedent-stress onset and CHDE onset. This linear formulation
525 did not capture potential nonlinear effects of antecedent stress. Future work could couple the
526 probability-based framework with process-based crop models to clarify nonlinear pathways through
527 which antecedent drought or heat affects compound hazard.

528 Second, we employed fixed thresholds for the identification of heat and drought events. Previous
529 studies indicated that when crops experienced antecedent drought (or heat) stress, their tolerance
530 thresholds to subsequent heat (or drought) stress shifted considerably (Qi 2025; Wang et al. 2023c). The
531 findings of this study further showed that CHDE in the study region rarely involved the simultaneous
532 onset of drought and heat. Instead, in most cases, a drought (or heat) event occurred first, followed by the
533 coupled onset of heat (or drought) stress, thereby forming a CHDE. Given this temporal misalignment of
534 CHDE, the use of static thresholds inevitably reduced the accuracy of exposure characterization, leading
535 to substantial deviations between assessed hazards and actual field-scale stress responses. Future research
536 should integrate dynamically evolving remote sensing vegetation indices or field-validated phenology
537 models to establish a stress discrimination system whose thresholds can be dynamically adjusted
538 according to both antecedent stress conditions and crop developmental stages. This improvement will
539 enhance both the reliability and the physical interpretability of CHDE hazard estimation.

5. Conclusions

This study developed a daily-scale hazard assessment framework to characterize CHDE hazard for rain-fed spring maize in the hilly region of Southwest China during 1961–2023. By integrating SPRI, EDD, antecedent drought and heat factors, and a copula-based duration–severity model, the framework captured short-duration compound events and the influence of antecedent stress. Results showed that drought-related antecedent factors dominated throughout the growing season, accounting for more than 69% of the total antecedent contribution and reaching 100% during the seedling stage; the relative contribution of heat-related antecedent factors was highest during R3–R6. CHDE hazard exhibited distinct stage-specific characteristics: events occurred most frequently during VE–V6 and R3–R6, whereas duration, severity, and the integrated hazard index were highest during R3–R6.

Compared with 1961–1992, CHDE during 1993–2023 occurred more frequently, lasted longer, and exhibited greater severity and higher hazard. High-hazard areas expanded from the eastern part of the study area toward the central and western regions. During R3–R6, the mean hazard index was approximately 1.4 higher in 1993–2023 than in 1961–1992, while severity generally increased by 3–5 units, identifying this stage as the principal window for CHDE preparedness and management. The consistently high heat-event frequency and CHDE hazard observed during VE–V6 and R3–R6 indicate that heat events were a key contributor to CHDE hazard affecting maize. The identified hazard windows suggest prioritizing soil-moisture conservation and supplemental irrigation from V0 to R3, while strengthening heat mitigation and water-stress preparedness during R3–R6.

References

Bolan S, Padhye LP, Jasemizad T, Govarthanan M, Karmegam N, Wijesekara H, Amarasiri D, Hou D, Zhou P, Biswal BK, Balasubramanian R, Wang H, Siddique KHM, Rinklebe J, Kirkham MB, Bolan N (2024) Impacts of climate change on the fate of contaminants through extreme weather events. Sci Total Environ 909:168388. https://doi.org/10.1016/j.scitotenv.2023.168388

Cao Z-Y, Chen Z-H, Tang B, Zeng Q, Guo H-L, Huang W-H, Luo Y, Shen S, Zhou S-L (2024) The effects of sowing date on maize: Phenology, morphology, and yield formation in a hot subtropical monsoon region. Field Crop Res 309:109309. https://doi.org/10.1016/j.fcr.2024.109309

Chen C, Pang Y, Xu F, Guo X (2018) Risk assessment of drought on rice at different growth stages in Sichuan Province. Agricultural Research in the Arid Areas 36:184–193. https://doi.org/10.7606/j.issn.1000-7601.2018.06.28

570 Chen D, Guo Y, Zhao Y, Zhang J, Liu X, Tong Z, Zhao C (2024) Dynamic evolution characteristics and hazard
571 assessment of compound drought/waterlogging and low temperature events for maize. Sci Total
572 Environ 946:174427. https://doi.org/10.1016/j.scitotenv.2024.174427
573 Chen QL, Xu JW, Shi SW, Li X, Wang P (2013) Building Drought Index Based on AMSR-E Data - A Case
574 Study in Hilly Area of Central Sichuan Basin. Advanced Materials Research 781-784:2292–2295.
575 https://doi.org/10.4028/www.scientific.net/AMR.781-784.2292
576 Feng S, Hao Z, Zhang X, Hao F (2019) Probabilistic evaluation of the impact of compound dry-hot events
577 on global maize yields. Sci Total Environ 689:1228–1234.
578 https://doi.org/10.1016/j.scitotenv.2019.06.373
579 Feng S, Hao Z, Zhang X, Hao F (2021) Changes in climate-crop yield relationships affect risks of crop yield
580 reduction. Agric For Meteorol 304-305:108401.
581 https://doi.org/10.1016/j.agrformet.2021.108401
582 Guo Y, Lu X, Zhang J, Li K, Wang R, Rong G, Liu X, Tong Z (2022) Joint analysis of drought and heat events
583 during maize (Zea mays L.) growth periods using copula and cloud models: A case study of
584 Songliao Plain. Agric Water Manage 259:107238. https://doi.org/10.1016/j.agwat.2021.107238
585 Hamed R, Steinmann CB, Ma Q, Balanzategui D, Broadman E, Lesk C, Kornhuber K (2025) Amplified
586 agricultural impacts from more frequent and intense sequential heat events. Environ Res Lett
587 20:114001. https://doi.org/10.1088/1748-9326/ae06b8
588 Hao Z, Hao F, Xia Y, Feng S, Sun C, Zhang X, Fu Y, Hao Y, Zhang Y, Meng Y (2022) Compound droughts and
589 hot extremes: Characteristics, drivers, changes, and impacts. Earth-Sci Rev 235:104241.
590 https://doi.org/10.1016/j.earscirev.2022.104241
591 He Y, Zhao Y, Duan Y, Hu X, Fang J (2024) Projected Increase in Compound Drought and Hot Days over
592 Global Maize Areas under Global Warming. Water 16:621. https://doi.org/10.3390/w16040621
593 Hu J, Zhao X, Gu L, Liu P, Zhao B, Zhang J, Ren B (2023) The effects of high temperature, drought, and
594 their combined stresses on the photosynthesis and senescence of summer maize. Agric Water
595 Manage 289:108525. https://doi.org/10.1016/j.agwat.2023.108525
596 Huang Y, Wang J, He D, Tang J (2017) Temporal-spatial change in adverse meteorological conditions
597 during spring maize growth in Southwest China under climate warming. Resources Science
598 39:1753–1764. https://doi.org/10.18402/resci.2017.09.13
599 Jian H, Gao Z, Guo Y, Xu X, Li X, Yu M, Liu G, Bian D, Cui Y, Du X (2024) Supplemental irrigation mitigates

yield loss of maize through reducing canopy temperature under heat stress. Agric Water Manage 299:108888. https://doi.org/10.1016/j.agwat.2024.108888

Jing L, Weng B, Yan D, Zhang S, Bi W, Yan S (2023) The persistent impact of drought stress on the resilience of summer maize. Front Plant Sci 14:1016993. https://doi.org/10.3389/fpls.2023.1016993

Kuang X, Zhang Y, Huang Y, Cheng K (2024) Role of warming trend in occurrence of record-breaking high-temperature events in China during the past 40 years. Q J R Meteorol Soc 150:5621–5634. https://doi.org/10.1002/qj.4897

Kumwimba MN, Zhu B, Wang T, Yuan Z, Muyembe DK (2016) Metal Distribution and Contamination Assessment in Drainage Ditch Water in the Main Rice/Vegetable Area of Sichuan Hilly Basin. Bull Environ Contam Toxicol 96:248–253. https://doi.org/10.1007/s00128-015-1706-2

Li J, Wang Z, Wu X, Zscheischler J, Guo S, Chen X (2021) A standardized index for assessing sub-monthly compound dry and hot conditions with application in China. Hydrol Earth Syst Sci 25:1587–1601. https://doi.org/10.5194/hess-25-1587-2021

Li Q, Wang P, Li Y, Tang J, Li X, Zhang Y, Han D, Wang Q, Zhao Y, Yang Z (2025) Hazard assessment of compound drought and heat events on summer maize from agricultural and meteorological perspectives. Agric Water Manage 313:109479. https://doi.org/10.1016/j.agwat.2025.109479

Liang W, Liang H, Tett SFB, Lott FC, Zhu X, Qiao S, Xue H, Hu H, Wang K, Dong W (2025) Attribution of the 2023 extreme spring hot drought event in Southwest China: meteorological and agricultural perspectives. Environ Res Lett 20:074019. https://doi.org/10.1088/1748-9326/addd38

Lin S, Li H, Huang P, Duan X (2022) Characteristics of high temperature, drought and circulation situation in summer 2022 in China. Journal of Arid Meteorology 40:748–763. https://doi.org/10.11755/j.issn.1006-7639(2022)-05-0748

Liu M, Yin Y, Wang X, Ma X, Chen Y, Chen W (2022) More frequent, long-lasting, extreme and postponed compound drought and hot events in eastern China. Journal of Hydrology 614:128499. https://doi.org/10.1016/j.jhydrol.2022.128499

Liu T, Zhang Y, Guo B, Zhang S, Li X (2024) Substantial increase in future land exposure to compound droughts and heatwaves in China dominated by climate change. Journal of Hydrology 645:132219. https://doi.org/10.1016/j.jhydrol.2024.132219

Liu Z (2024) Research on the effects of combined temperature and water stress on summer maize yield

in the north China Plain based on Vine copula function. Master's thesis, Nanjing University of Information Science and Technology, Nanjing. https://doi.org/10.27248/d.cnki.gnjqc.2024.000552

Liu Z, Qiu R, Zhang Q (2025) Differences in effects of varying compound extreme temperature and precipitation events on summer maize yield in North China. Agric Water Manage 307:109237. https://doi.org/10.1016/j.agwat.2024.109237

Luan X, Vico G (2021) Canopy temperature and heat stress are increased by compound high air temperature and water stress and reduced by irrigation – a modeling analysis. Hydrol Earth Syst Sci 25:1411–1423. https://doi.org/10.5194/hess-25-1411-2021

Meena B, Kavita, Kumar A, Roy DK (2024) Effect of individual and combination of heat and drought stress in maize at reproductive and grain filling stage. Plant Physiol Rep 29:889–902. https://doi.org/10.1007/s40502-024-00832-1

Pan X, Wang W, Shao Q, Wei J, Li H, Zhang F, Cao M, Yang L (2024) Compound drought and heat waves variation and association with SST modes across China. Sci Total Environ 907:167934. https://doi.org/10.1016/j.scitotenv.2023.167934

Qi Y (2025) Study on the impact mechanisms of high temperature and drought on maize growth and the disaster thresholds in arid and semi-arid regions. PhD thesis, Lanzhou University, Lanzhou. https://doi.org/10.27204/d.cnki.glzhu.2025.000180

Qian C, Ye Y, Jiang J, Zhong Y, Zhang Y, Pinto I, Huang C, Li S, Wei K (2024) Rapid attribution of the record-breaking heatwave event in North China in June 2023 and future risks. Environ Res Lett 19:014028. https://doi.org/10.1088/1748-9326/ad0dd9

Qu Z, Yao S, Liu D (2024) Response of drought to climate extremes in a semi-arid inland river basin in China. J Arid Land 16:1505–1521. https://doi.org/10.1007/s40333-024-0064-5

Riedesel L, Ma D, Piepho H-P, Laidig F, Möller M, Golla B, Kautz T, Feike T (2024) Climate change induced heat and drought stress hamper climate change mitigation in German cereal production. Field Crop Res 317:109551. https://doi.org/10.1016/j.fcr.2024.109551

Shi P, Li Y, Biswas A, Wei K, Hou M (2024) Spatial-temporal evolution and intrinsic drivers of compound drought and heatwave events in Mainland China. Sci Total Environ 948:174834. https://doi.org/10.1016/j.scitotenv.2024.174834

Song X, Chen H, Chen T, Huang Q, Deng S, Yang N (2024) Spatial and temporal variations of spring

drought in Southwest China and its possible teleconnection with the global climate events. Journal of Hydrology: Regional Studies 51:101655. https://doi.org/10.1016/j.ejrh.2024.101655

Vogel E, Donat MG, Alexander LV, Meinshausen M, Ray DK, Karoly D, Meinshausen N, Frieler K (2019) The effects of climate extremes on global agricultural yields. Environ Res Lett 14:054010. https://doi.org/10.1088/1748-9326/ab154b

Wang A, Tao H, Ding G, Zhang B, Huang J, Wu Q (2023a) Global cropland exposure to extreme compound drought heatwave events under future climate change. Weather Clim Extremes 40:100559. https://doi.org/10.1016/j.wace.2023.100559

Wang H, Zhang G, Zhang S, Shi L, Su X, Song S, Feng K, Zhang T, Fu X (2023b) Development of a novel daily-scale compound dry and hot index and its application across seven climatic regions of China. Atmos Res 287:106700. https://doi.org/10.1016/j.atmosres.2023.106700

Wang L, Liao S, Huang S, Ming B, Meng Q, Wang P (2018a) Increasing concurrent drought and heat during the summer maize season in Huang–Huai–Hai Plain, China. Int J Climatol 38:3177–3190. https://doi.org/10.1002/joc.5492

Wang M (2012) Trends and response measures of agricultural seasonal drought under climate change in Sichuan. PhD thesis, Sichuan Agricultural University, Ya'an.

Wang N, Wang E, Wang J, Zhang J, Zheng B, Huang Y, Tan M (2018b) Modelling maize phenology, biomass growth and yield under contrasting temperature conditions. Agric For Meteorol 250-251:319–329. https://doi.org/10.1016/j.agrformet.2018.01.005

Wang R, Zhao H, Qi Y, Zhao F, Chen F, Ding W, Jiang J, Zhang K, Wang H (2023c) Onset and severity thresholds of drought impacts on wheat. Agric Water Manage 281:108259. https://doi.org/10.1016/j.agwat.2023.108259

Wang W, Zhang Y, Guo B, Ji M, Xu Y (2021) Compound droughts and heatwaves over the Huai River Basin of China: From a perspective of the magnitude index. J Hydrometeorol 22:3107–3119. https://doi.org/10.1175/jhm-d-20-0305.1

Wang X, Lang X, Jiang D (2024) Human activities increased compound drought and heat events over China during 1961–2014. Int J Climatol 44:5090–5103. https://doi.org/10.1002/joc.8625

Wang Y, Wang Y, Chen Y, Chen H, Li X, Ding Z, Han X, Tang X (2023d) Spatial and Temporal Characteristics of Drought Events in Southwest China over the Past 120 Years. Remote Sens 15:3008. https://doi.org/10.3390/rs15123008

690 Wang Y, Wang J, Gong D, Ding M, Zhong W, Deng M, Kang Q, Ding Y, Liu Y, Zhang J (2025) Spatiotemporal
691 Heterogeneity and Zonal Adaptation Strategies for Agricultural Risks of Compound Dry and Hot
692 Events in China's Middle Yangtze River Basin. Remote Sens 17:2892.
693 https://doi.org/10.3390/rs17162892
694 Wei X, Huang S, Liu D, Li J, Huang Q, Leng G, Shi H, Peng J (2024) The response of agricultural drought to
695 meteorological drought modulated by air temperature. Journal of Hydrology 639:131626.
696 https://doi.org/10.1016/j.jhydrol.2024.131626
697 Wu H, Su X, Singh VP, Niu J (2024) Predicting compound agricultural drought and hot events using a
698 Cascade Modeling framework combining Bayesian Model Averaging ensemble with Vine Copula
699 (CaMBMAViC). Journal of Hydrology 642:131901. https://doi.org/10.1016/j.jhydrol.2024.131901
700 Wu X, Hao Z, Zhang X, Li C, Hao F (2020) Evaluation of severity changes of compound dry and hot events
701 in China based on a multivariate multi-index approach. Journal of Hydrology 583:124580.
702 https://doi.org/10.1016/j.jhydrol.2020.124580
703 Xiang X, Li Y, Wu X, Cao H, Lin X (2024) Delineating the predominant impact of rising temperature on the
704 enhancement of severity in compound drought-hot events in China: An empirical Copula and
705 path analysis-based approach. Journal of Hydrology: Regional Studies 53:101769.
706 https://doi.org/10.1016/j.ejrh.2024.101769
707 Xiao H, Xu P, Wang L (2024) The Unprecedented 2023 North China Heatwaves and Their S2S
708 Predictability. Geophys Res Lett 51:e2023GL107642. https://doi.org/10.1029/2023gl107642
709 Xu P, Wang D, Wang Y, Singh VP, Qiu J, Wu J, Zhang A, Ju X (2023) +Dynamic identification and risk
710 analysis of compound dry-hot events considering nonstationarity. Journal of Hydrology
711 616:128852. https://doi.org/10.1016/j.jhydrol.2022.128852
712 Xue Y, Chen Q, Zhang J, Huang P (2020) Trends in extreme high temperature at different altitudes of
713 Southwest China during 1961-2014. Atmos Ocean Sci Lett (UK) 13:417–425.
714 https://doi.org/10.1080/16742834.2020.1799689
715 Yang J, Wu J, Zhou L, Zhou H, Zhang Z, Zhang R (2025) Characteristics of compound heat and drought
716 events during the spring maize growing season in Northeast China Based on a novel daily-scale
717 analysis framework. Journal of Hydrology: Regional Studies 57:102140.
718 https://doi.org/10.1016/j.ejrh.2024.102140
719 Yang Y, Li K, Wei S, Guga S, Zhang J, Wang C (2022) Spatial-temporal distribution characteristics and

720 hazard assessment of millet drought disaster in Northern China under climate change. Agric
721 Water Manage 272:107849. https://doi.org/10.1016/j.agwat.2022.107849
722 Yu H, Zhou C, Chen C, Chen Y (2023) Analysis of atmospheric circulation background and main impacts of
723 heatwave in Sichuan Basin from July to August 2021. Journal of Arid Meteorology 41:923–932.
724 https://doi.org/10.11755/j.issn.1006-7639(2023)-06-0923
725 Yu R, Zhai P (2020) More frequent and widespread persistent compound drought and heat event
726 observed in China. Sci Rep 10:14576. https://doi.org/10.1038/s41598-020-71312-3
727 Yu R, Dong S, Han Z, Li W (2024) Increased exposure of rice to compound drought and hot extreme
728 events during its growing seasons in China. Ecol Indic 167:112735.
729 https://doi.org/10.1016/j.ecolind.2024.112735
730 Zhang S, Qi G, Su K, Zhou L, Bai H (2022a) Research on Sequence Construction and Characteristics
731 Diagnosis of Droughts and Floods in the Qinling Mountains of China From 1850 to 1959. Front
732 Earth Sci 10:860750. https://doi.org/10.3389/feart.2022.860750
733 Zhang Y, Guo L, Liang C, Zhao L, Wang J, Zhan C, Jiang S (2022b) Encounter risk analysis of crop water
734 requirements and effective precipitation based on the copula method in the Hilly Area of
735 Southwest China. Agric Water Manage 266:107571.
736 https://doi.org/10.1016/j.agwat.2022.107571
737 Zhang Y, Hao Z, Zhang Y (2023a) Agricultural risk assessment of compound dry and hot events in China.
738 Agric Water Manage 277:108128. https://doi.org/10.1016/j.agwat.2022.108128
739 Zhang Y, Wang P, Chen Y, Yang J, Wu D, Ma Y, Huo Z, Liu S (2023b) The optimal time-scale of Standardized
740 Precipitation Index for early identifying summer maize drought in the Huang-Huai-Hai region,
741 China. Journal of Hydrology: Regional Studies 46:101350.
742 https://doi.org/10.1016/j.ejrh.2023.101350
743 Zhao Q, Zhang X, Li C, Xu Y, Fei J (2024) Compound ecological drought assessment of China using a
744 Copula-based drought index. Ecol Indic 164:112141.
745 https://doi.org/10.1016/j.ecolind.2024.112141
746 Zheng Y, Zhang T, Yang S, Jiang X, Luo Y, Yan H, Deng K, Zhang C (2025) Changes in Teleconnection
747 Patterns and Land–Atmosphere Coupling Amplify the Spring–Early Summer Heatwaves Over
748 Southwestern China. Int J Climatol 45:e8732. https://doi.org/10.1002/joc.8732
749 Zhi F, Zhang J, Bao Y, Bao Y, Dong Z, Tong Z, Liu X (2024) Assessment of waterlogging hazard during maize

growth stage in the Songliao plain based on daily scale SPEI and SMAI. Agric Water Manage 304:109081. https://doi.org/10.1016/j.agwat.2024.109081

Zhou C, Wang G, Jiang H, Li S, Shi X, Hu Y, Cabral P (2025) Spatio-temporal patterns of compound dry-hot extremes in China. Atmos Res 314:107795. https://doi.org/10.1016/j.atmosres.2024.107795

Zhu B, Wang T, Kuang F, Luo Z, Tang J, Xu T (2009) Measurements of Nitrate Leaching from a Hillslope Cropland in the Central Sichuan Basin, China. Soil Sci Soc Am J 73:1419–1426. https://doi.org/10.2136/sssaj2008.0259

Zhu X, Liu Y, Xu K, Pan Y (2021a) Effects of Drought on Vegetation Productivity of Farmland Ecosystems in the Drylands of Northern China. Remote Sens 13:1179. https://doi.org/10.3390/rs13061179

Zhu X, Zhang S, Liu T, Liu Y (2021b) Impacts of Heat and Drought on Gross Primary Productivity in China. Remote Sens 13:378. https://doi.org/10.3390/rs13030378

Zhu X, Liu T, Xu K, Chen C (2022) The impact of high temperature and drought stress on the yield of major staple crops in northern China. J Environ Manage 314:115092. https://doi.org/10.1016/j.jenvman.2022.115092

Statements & Declarations

Funding

This work was supported by the National Key Research and Development Program of China (Grant No. 2024YFD2301305 to Yufang Zhang) and the National Natural Science Foundation of China (Grant No. 52109060 to Lu Zhao).

Declaration of competing interests

The authors declare that they have no known competing financial interests or personal relationships that could have appeared to influence the work reported in this paper.

Author Contributions

Yang Yang: Methodology, Validation, Formal analysis, Data curation, Writing – original draft, Visualization. Lu Zhao: Conceptualization, Methodology, Resources, Writing – review & editing, Visualization, Funding acquisition. Shouzheng Jiang: Conceptualization, Validation, Formal analysis, Supervision. Cun Zhan: Writing – review & editing, Visualization, Supervision. Ningbo Cui: Validation, Supervision, Project administration. Yufang Zhang: Project administration, Funding acquisition. Ziyi Liu: Software, Data curation, Visualization. Ziqi Song: Software, Data curation. Hanyue Li: Data curation. All authors commented on previous versions of the manuscript and read and approved the final version.

Data Availability Statement

Daily meteorological data for 1961–2023 were obtained from the China Meteorological Data Service Center (http://data.cma.cn). Spring maize phenological records were compiled from provincial statistical yearbooks and published studies, and crop coefficients were adopted from Wang (2012). The processed datasets supporting the findings of this study are available from the corresponding author upon reasonable request.